

End-to-End Propagation Noise and Memory Analysis for Molecular Communication over Microfluidic Channels

A. Ozan Bicen, *Student Member, IEEE*, and Ian F. Akyildiz, *Fellow, IEEE*

Abstract—Molecular communication (MC) between a transmitter and a receiver placed in the chambers attached to a microfluidic channel is investigated. A linear end-to-end channel model is developed capturing the effects of the diffusion and the junction transition at the chambers, as well as the microfluidic channel shapes and the fluid flow. The spectral density of the propagation noise is studied, and the flat frequency bands are identified for the chambers and the microfluidic channel. This suggests that in certain microfluidic design choices, the spectral density of noise may end up naturally being flat. Motivated by this result, the additive white Gaussian noise (AWGN) model is developed based on the chamber, the microfluidic channel, and the fluid flow parameters for the end-to-end propagation noise. Furthermore, the molecular memory is modeled due to inter-diffusion among transmitted molecular signals. The effect of the molecular memory on the end-to-end propagation noise is also analyzed. To substantiate our analytical results, the ranges of physical parameters that yield a linear end-to-end MC channel are investigated. These results show the validity of the AWGN model for MC over microfluidic channels and characterize the impact of the microfluidic channel and chamber geometry on the propagation noise and memory.

Index Terms—Molecular communication, microfluidics, noise, channel models, Gaussian channels, memory.

I. INTRODUCTION

MOLECULAR COMMUNICATION (MC) is a nanoscale paradigm that relies on transport of molecules to enable sensing and detection in microenvironments [1], [2]. It provides advantages for biochemical signal sensing including higher accuracy, high-throughput analysis, compactness, point-of-care diagnostics, and extraction of localized features at nanoscale in biological environments and lab-on-a-chip systems. To realize these potential gains and design efficient yet practical MC systems, the understanding of the mass transport mechanisms behind the molecular signal propagation from the transmitter to the receiver is imperative.

Microfluidics provides opportunity to automatize the chemistry and biology fields by performing various experiments swiftly and in parallel while consuming small amount of

Manuscript received July 25, 2013; revised February 22, 2014; accepted May 8, 2014. Date of publication May 13, 2014; date of current version July 18, 2014. This work was supported by the U.S. National Science Foundation under Grant CNS-1110947. The associate editor coordinating the review of this paper and approving it for publication was O. B. Akan.

The authors are with the Broadband Wireless Networking Laboratory, School of Electrical and Computer Engineering, Georgia Institute of Technology, Atlanta, GA 30332 USA (e-mail: bozan@ece.gatech.edu; ian@ece.gatech.edu).

Digital Object Identifier 10.1109/TCOMM.2014.2323293

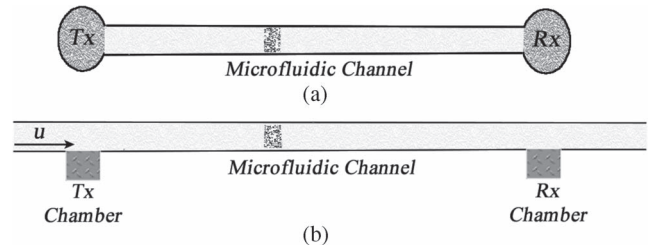


Fig. 1. Propagation of concentration signal from transmitter (Tx) and receiver (Rx) patches through the microfluidic channel without (a) and with (b) flow.

reagent [3]–[5]. Microfluidic chips can be utilized to develop test-beds for and applications of MC via creating habitats for molecular transmitter and receiver such as a bacteria population [6], [7]. An MC system is given in Fig. 1(a) where molecular transmitter and receiver patches are connected via a microfluidic channel. Biochemical samples can be supplied to the transmitter bacteria to start a chain of reactions for detection and separation purposes, and the receiver can participate in automated multi-stage chemical assays. Furthermore, the flowing fluid inside the microfluidic channel can be utilized to enhance the propagation of the transmitted, i.e., released, concentration of the molecules. Specifically, we target an MC system where the molecular transmitter and receiver are placed in chambers and communicate over a microfluidic channel containing fluid flow, i.e., Flow-induced Molecular Communication (FMC), as shown in Fig. 1(b).

The analysis of the noise effects for undergoing mass transport mechanisms at the chambers and the microfluidic channel is essential to facilitate development of efficient and practical MC techniques. So far, the propagation modeling and the chemical noise analysis for transmitter and receiver for MC have been a research focus in recent years [8]–[10]. The noise effects on the diffusion-based concentration signal propagation in a free space MC system are studied in [11], under the assumption that the molecules propagate from the transmitter to the receiver solely via diffusion. Furthermore, the utilization of the microfluidic channels with fluid flow for FMC is investigated in [12]. While the microfluidic channels with fluid flow enhances the propagation of concentration signal, the FMC paradigm necessitates a new propagation noise notion. This new notion should address the noise effects on the received signal: 1) transition from/to molecular transport by diffusion in the transmitter/receiver chamber to/from molecular transport by flow in the microfluidic channel; and 2) the random diffusion of

molecules inside the chambers and microfluidic channel. Additionally, the investigation of the molecular memory effect due to self-interference created by diffusion of molecules between the transmitted molecular signals is vital.

Our work is motivated by the fact that an efficient FMC system can be devised when the noise and memory effects are understood and predicted by using the developed analytic framework. The notion of controlling the noise and memory effects for efficient FMC via design of chambers and microfluidic channels distinguishes our work from other existing noise analyses that solely focus on identification of noise sources and developing models on top of them [10], [11]. To the best of our knowledge, the noise and memory effects in MC have not been studied from this perspective before.

In this paper, first, the propagation model presented in [12] is extended, and a linear end-to-end model incorporating the propagation through the chambers is proposed. Then, the building blocks of the propagation noise is developed based on the autocorrelation function of the molecular signal under the effects of the transition from chamber to microfluidic channel, and vice versa, at junctions, and the diffusion at the chambers and microfluidic channel. Spectral densities of the propagation noise for the transmitter chamber, the microfluidic channel, and the receiver chamber are formulated. Frequency ranges at which spectral density of noise is flat-band are investigated based on the chamber, microfluidic channel, and flow parameters. An Additive White Gaussian Noise (AWGN) model is proposed for FMC in accordance with the flat-band frequency range in the spectral density of the end-to-end propagation noise. Furthermore, the memory due to the diffusion of transmitted molecular signal is analyzed. The statistical properties of the received memory component is studied based on the transmission, the transmitter/receiver chamber, the microfluidic channel, and the fluid flow parameters. Moreover, the effect of molecular memory on end-to-end propagation noise is revealed. Some of the salient features of this study are listed as follows:

- **An Analysis of the Propagation Noise:** Building blocks for the spectral density of the propagation noise are defined. The end-to-end propagation noise is obtained based on the spectral density of noise at the transmitter chamber, the microfluidic channel, and the receiver chamber. AWGN model for the FMC paradigm is developed.
- **A Linear Molecular Memory Model:** The memory effect due to inter-diffusion of the previously transmitted molecules signals inside microfluidic channel and chambers is analyzed. The memory level is characterized based on the transmission frequency and the distance. The amplitude and the variance of the memory component in the received signal is derived based on the FMC system parameters. Furthermore, the effect of memory on molecular noise is studied, and the end-to-end propagation noise is extended to include this effect.

These are the truly novel aspects of our work and are the main contribution of the proposed analysis of the propagation noise and the memory for MC over microfluidic channels.

The remainder of the paper is organized as follows. In Section II, we present a review of related work on noise analy-

sis. We present the propagation model for FMC in Section III. The building blocks of noises in FMC are formulated, and noise spectrum is investigated in Section IV. In Section V, molecular memory analysis is presented. Numeric results are presented in Section VI. Finally, the paper is concluded in Section VII.

II. RELATED WORK

The molecular transport over microfluidic channels is investigated in depth in many papers in the last decade [13]–[19] where the microfluidic device aspects are explored in depth for the concentration propagation via diffusion and flow, i.e., convection. These contributions aim to find the optimum device parameters to shape the input concentration through the microfluidic channels. More recently, the generation of the higher harmonics of the input concentration wave is investigated based on the microfluidic channel parameters and the interconnection of microfluidic channels [20]. However, the utilization of concentration as a signal for communication between a transmitter and receiver pair is not considered. As a consequence, none of the above studies investigate the noise or memory effects on the concentration signal in microfluidic channels to empower the FMC systems.

On the other hand, there was an extensive research effort on propagation modeling for MC in recent years [8], [12], [21]. For example, solutions have been proposed independent from noise and memory effects for solely diffusion-based free space concentration propagation [8]. Although the investigation of molecular signaling based on the diffusion and convection mechanisms is extremely important, the research on the noise and memory effects is vital to design efficient yet practical FMC systems. In [11], the molecular noise is studied for a diffusion-based MC system. However, the effects of fluid flow, the chamber, and the microfluidic channel parameters on molecular noise have not been investigated so far. In [10], the noise analysis is performed on the receiver side neglecting molecular noise effects and assuming a specific chemical receiver architecture based on receptor-ligand kinetics. Additionally, MC using individual molecules is studied based on simulation experiments without analytic formulation under ideal transmitter and diffusion-based propagation assumptions [22], [23].

In contrast, in our paper we present the propagation noise and memory effects for an FMC system, where the transmitter and the receiver chambers are connected via the microfluidic channel with the fluid flow. The microfluidic channel configurations that yield flat-band noise spectral density are investigated, and the design principles for physical parameters of the MC system to have a valid linear MC model are highlighted.

III. END-TO-END MOLECULAR PROPAGATION IN FMC

In the following discussions, we formally define the physical model of the molecular communication over microfluidic channels. Before proceeding to the analysis of the propagation noise and the memory effects on the received concentration signal, we introduce the notion of the transmitter and the receiver chambers, and develop a linear end-to-end model for the propagation of the released molecules from the transmitter in

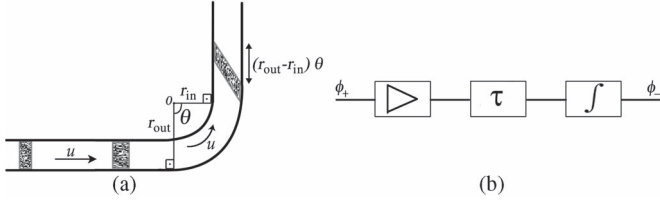


Fig. 2. Molecular propagation inside the turning microfluidic channel with angle θ (a) and block diagram representation (b).

the transmitter chamber to the receiver in the receiver chamber. We also incorporate the delays, and the transfer functions for the transmitter and the receiver chambers into the developed end-to-end model, and set the stage for the noise and memory analysis by defining the noise and the memory effects on the concentration signal.

A. Physical Model

Consider the typical MC applications involving the sensing of the chemical signals by the transmitter, and communication of event features with the receiver. We assume that the molecular transmitter and receiver are placed in transmitter and receiver chambers, respectively, which are connected via a microfluidic channel with fluid flow, as shown in Fig. 1(b). The main rationale behind such a flow-induced molecular communication notion is that the propagation of the input concentration signal ϕ_+ generated by the transmitter is enhanced by the fluid flow, which alleviates dispersion of the molecules, i.e., path-loss, and propagation time, i.e., the delay τ , of the received concentration signal ϕ_- . The transmitter and the receiver chambers contain the application specific molecular systems such as a bacteria population [6]. The transmitter generates a concentration signal to communicate the features of the sensed chemical event with the receiver. Here, our focus is on the molecular transport, i.e., the propagation, the mechanisms, hence, the specifics of such a concentration generation process based on chemical kinetics are application dependent and beyond the scope of our paper.

In fact, the impulse response, the delay, and the transfer function for molecular propagation in microfluidic channels are derived as functions of the channel length l_{ch} , height a_{ch} , width b_{ch} , turning angle θ , and pressure drop across the channel Δp in [12]. The fluid flow in the microfluidic channel is taken to be laminar, steady, unidirectional, and driven by the pressure drop across the microfluidic channel [24]. The area-averaged flow velocity u for a rectangular cross-section microfluidic channel is given by [25]

$$u = \frac{a_{ch}^2}{12\mu l_{ch}} \left(1 - 0.63 \frac{a_{ch}}{b_{ch}} \right) \Delta p \quad (1)$$

where μ is the viscosity of the fluid. We also assume that due to very short distance in the order of $\sim \mu m$ at transmitter and receiver chambers, propagation velocity by diffusion at chambers is comparable to propagation via flow in microfluidic channel. One-dimensional solution of the convection-diffusion equation is used to analyze molecular transport via flow in the microfluidic channels [13]–[17]. The concentration propagation in the microfluidic channel is illustrated in Fig. 2(a).

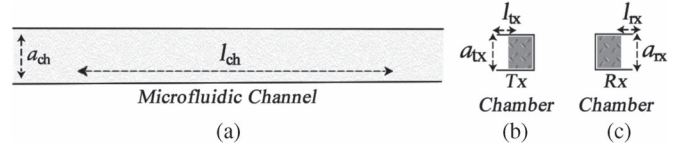


Fig. 3. The illustration of length l_{ch} , l_{tx} , and l_{rx} parameters and height a_{ch} , a_{tx} , and a_{rx} parameters for the microfluidic channel (a), the transmitter chamber (b), and the receiver chamber (c), respectively.

In the turning channels, the inner and the outer radius of the microfluidic channel, i.e., r_{in} and r_{out} , are different, which causes different laminas to travel different lengths. The cross-section of the microfluidic channel is invariant, and hence, the difference $r_{out} - r_{in}$ is equal to a_{ch} . The impulse response of the turning channel, i.e., $\theta > 0$, is given by [12]

$$h_{ch}(l) = \frac{1}{a_{ch}\theta} \int_0^{a_{ch}\theta} \frac{1}{\sqrt{4\pi D\tau_{ch}}} e^{-\frac{(l-u\tau_{ch}+x')^2}{4D\tau_{ch}}} dx' \quad (2)$$

where the height a_{ch} , and length l_{ch} parameters are illustrated in Fig. 3(a), τ_{ch} is given by $\tau_{ch} = (l_{ch} + a_{ch}\theta)/u$, which is the average delay based on the symmetry around central lamina in the turning channel, and D is the effective diffusion coefficient adjusted according to the Taylor dispersion in rectangular channels based on the intrinsic molecular diffusion coefficient D_0 as [26]

$$D = \left(1 + \frac{8.5u^2 a_{ch}^2 b_{ch}^2}{210D_0^2 (a_{ch}^2 + 2.4a_{ch}b_{ch} + b_{ch}^2)} \right) D_0. \quad (3)$$

The turning microfluidic channel depicted in Fig. 2(a) can be seen as an integrator due to its impulse response, which is also a low-pass filter. The impulse response of a straight microfluidic channel, i.e., $\theta = 0$, is given by

$$\begin{aligned} h_{ch}^{str}(l) &= \lim_{\theta \rightarrow 0} \frac{1}{a_{ch}\theta} \int_0^{a_{ch}\theta} \frac{1}{\sqrt{4\pi D\tau_{ch}}} e^{-\frac{(l-u\tau_{ch}+x')^2}{4D\tau_{ch}}} dx' \\ &= \frac{1}{\sqrt{4\pi D\tau_{ch}}} e^{-\frac{(l-u\tau_{ch})^2}{4D\tau_{ch}}}. \end{aligned} \quad (4)$$

Furthermore, the transfer function of the turning microfluidic channel is found by taking the Fourier Transform of (2) and expressed using normalized sinc function as

$$H_{ch}(k) = e^{-(k^2 D + jku)\tau_{ch}} \text{sinc} \left(\frac{a_{ch}\theta}{2\pi} k \right) e^{-jk a_{ch}\theta/2} \quad (5)$$

where k is the angular spatial frequency, i.e., wave number. The transfer function $H_{ch}(k)$ can be simplified for a straight channel using $\theta = 0$ as

$$H_{ch}^{str}(k) = e^{-(k^2 D + jku)\tau_{ch}}. \quad (6)$$

Overall, the molecular propagation inside microfluidic channel can be represented using block diagrams via a series connection of attenuator, delay, and integrator elements, as depicted in Fig. 2(b). Next, we model the concentration propagation in the chambers, and the effect of transition at the junctions to/from the microfluidic channel from the transmitter chamber and to the receiver chamber, respectively.

B. Impact of the Chambers on the Molecular Propagation

The received concentration signal can be obtained via convolution of the input signal with the transmitter, the microfluidic channel, and the receiver impulse responses. Although, the concentration propagation in the microfluidic channel is investigated in [12], the impulse responses, the transfer functions, and the delays of the transmitter and the receiver chambers are yet to be explored. Here, we provide a model including molecular propagation in chambers as well as from/to chambers to/from microfluidic channel at the junctions.

1) *Transmitter Chamber:* To model the concentration propagation in the transmitter chamber, the solution of the diffusion equation for a point source placed in the chamber, i.e., impulse response, is used. The diffusion equation is defined as [25]

$$\frac{\partial \phi}{\partial \tau} = D_0 \frac{\partial^2 \phi}{\partial l^2} \tag{7}$$

which relates the variation of concentration in time domain to variation of concentration in space domain. The solution of the diffusion equation for a point source input, i.e., $\phi_+(l) = \delta(l)$; where δ is the Dirac delta function, is given by

$$h'_{tx}(l) = \frac{1}{\sqrt{4\pi D_0 \tau_{tx}}} e^{-\frac{l^2}{4D_0 \tau_{tx}}} \tag{8}$$

where τ_{tx} is the delay at the transmitter chamber, which is calculated based on the travel time of peak level of concentration, i.e., $\max_{\tau_{tx}} \|\phi\|$ via setting

$$\left. \frac{\partial h'_{tx}}{\partial \tau_{tx}} \right|_{l=l_{tx}} = 0 \tag{9}$$

which gives

$$\frac{l_{tx}^2 - 2D_0 \tau_{tx}}{8\sqrt{\pi}(D_0 \tau_{tx})^{5/2}} D_0 e^{-\frac{l_{tx}^2}{4D_0 \tau_{tx}}} = 0 \tag{10}$$

from which τ_{tx} is found as

$$\tau_{tx} = \frac{l_{tx}}{2D_0}. \tag{11}$$

Due to the finite size height a_{tx} of the transmitter chamber, which is illustrated in Fig. 3(b), the transmitted concentration signal has a pulse width as large as the chamber height a_{tx} at the junction between the transmitter chamber and the microfluidic channel, where the center of the transmitter junction is taken as the origin of the transmitter coordinate axis. The impulse response of a such behavior, i.e., the junction impulse response, is captured by a scaled rect function to match the chamber height as

$$h_{tx}^{jct}(l) = \frac{1}{a_{tx}} \text{rect} \left(\frac{1}{a_{tx}} l - \frac{1}{2} \right) \tag{12}$$

where the signal is shifted by half chamber height $a_{tx}/2$ to keep system causality, and $\text{rect}(l)$ is

$$\text{rect}(l) = \begin{cases} 1, & |l| \leq 1/2 \\ 0, & |l| > 1/2. \end{cases}$$

The delay due to shifting of the signal, i.e., $a_{tx}/(2u)$, is incorporated into microfluidic channel delay in Section III-C.

The overall impulse response of transmitter chamber is formulated as

$$\begin{aligned} h_{tx}(l) &= \left(h_{tx}^{jct} * h'_{tx} \right) (l) \\ &= \frac{1}{a_{tx}} \int_0^{a_{tx}} \frac{1}{\sqrt{4\pi D \tau_{tx}}} e^{-\frac{(l-x)^2}{4D \tau_{tx}}} dx \end{aligned} \tag{13}$$

where τ_{tx} is as given in (11). For a transmitter chamber with a height of $a_{tx} = 0$, the impulse response of the transmitter chamber reduces to (8). The transfer function for transmitter chamber H_{tx} is found by taking Fourier Transform of the impulse response, i.e., $\mathcal{F}\{h_{tx}\}$, and using normalized sinc function as

$$H_{tx}(k) = e^{-k^2 D \tau_{tx}} \text{sinc} \left(\frac{a_{tx}}{2\pi} k \right) e^{-jk a_{tx}/2}. \tag{14}$$

2) *Receiver Chamber:* Similar to the transmitter chamber, for the concentration propagation in the receiver chamber, we also utilize the solution of the diffusion (7) for a point source according to the receiver chamber parameters, i.e., the receiver chamber length l_{rx} , and the receiver chamber height a_{rx} . The receiver chamber performs as an integrator during the transition of concentration from the microfluidic channel to the chamber, whose behavior can be captured by an auxiliary rect function similar to transmitter side (12), where the center of the receiver junction is taken as the origin of the receiver coordinate axis, and hence, the concentration signal is shifted by half chamber height $a_{rx}/2$ to achieve causality, as

$$h_{rx}^{jct}(l) = \frac{1}{a_{rx}} \text{rect} \left(\frac{1}{a_{rx}} l - \frac{1}{2} \right). \tag{15}$$

The delay due to shifting of the signal, i.e., $a_{rx}/(2u)$, is incorporated into the microfluidic channel delay in Section III-C. Using the solution of the diffusion equation at the transmitter chamber for a point source in (8), the impulse response for the concentration propagation in the receiver chamber is obtained as

$$h'_{rx}(l) = \frac{1}{\sqrt{4\pi D_0 \tau_{rx}}} e^{-\frac{l^2}{4D_0 \tau_{rx}}}. \tag{16}$$

The impulse response of the receiver chamber incorporating the effect of the receiver junction is formulated as

$$\begin{aligned} h_{rx}(l) &= \left(h'_{rx} * h_{rx}^{jct} \right) (l) \\ &= \frac{1}{a_{rx}} \int_0^{a_{rx}} \frac{1}{\sqrt{4\pi D_0 \tau_{rx}}} e^{-\frac{(l-x)^2}{4D_0 \tau_{rx}}} dx \end{aligned} \tag{17}$$

where the delay of the receiver chamber τ_{rx} can be obtained by solving (10) for the receiver chamber as

$$\tau_{rx} = \frac{l_{rx}}{2D_0}. \tag{18}$$

Similar to the transmitter chamber case, it is observed that for a receiver chamber with a height of $a_{rx} = 0$, the impulse response

of the transmitter chamber reduces to (16). Finally, the transfer function of the receiver chamber is given by $\mathcal{F}\{h_{rx}\}$ as

$$H_{rx}(k) = e^{-(k^2 D + jku)\tau_{rx}} \text{sinc}\left(\frac{a_{rx}}{2\pi}k\right) e^{-jk a_{rx}/2}. \quad (19)$$

Overall, the impulse responses, the delays, and the transfer functions are provided for the chambers and the microfluidic channel. Next, we propose the linear end-to-end model for FMC and identify the noise and memory effects on the end-to-end signal propagation.

C. Linear End-to-End Signal Model

The transmitted molecular signal ϕ_+ can be represented by

$$\phi_+(l) = m(l)e^{j2k_0 l} \quad (20)$$

where k_0 is the carrier frequency of the molecular oscillators placed in the transmitter and receiver chambers, $m(l)$ is the message signal, which is a wide-sense stationary process subject to variance constraint ψ^2 as

$$E[m^2(l)] = \psi^2. \quad (21)$$

For signal reception, we consider the propagation of the leading edge of the molecular signal at carrier frequency k_0 . Therefore, for MC channel response, gain of the system is calculated for a delay of τ_{tx} , τ_{ch} , and τ_{rx} in transmitter chamber, microfluidic channel, and receiver chamber, respectively. The signal gain at the transmission frequency k_0 and delay τ_{tx} for the transmitter chamber α_{tx} is found using Wiener-Khinchin theorem as

$$\begin{aligned} \alpha_{tx} &= |H_{tx}(k_0)| \\ &= \exp(-k_0^2 D_0 \tau_{tx}) \text{sinc}\left(\frac{a_{tx}}{2\pi}k_0\right). \end{aligned} \quad (22)$$

For the microfluidic channel, the signal gain at the transmission frequency k_0 and delay τ_{ch} , is found as

$$\begin{aligned} \alpha_{ch} &= |H_{ch}(k_0)| \\ &= \exp(-k_0^2 D \tau_{ch}) \text{sinc}\left(\frac{a_{ch}\theta}{2\pi}k_0\right). \end{aligned} \quad (23)$$

For the receiver chamber, the signal gain at the transmission frequency k_0 and delay τ_{rx} is found as

$$\begin{aligned} \alpha_{rx} &= |H_{rx}(k_0)| \\ &= \exp(-k_0^2 D_0 \tau_{rx}) \text{sinc}\left(\frac{a_{rx}}{2\pi}k_0\right). \end{aligned} \quad (24)$$

Combining the attenuation at the chambers and the microfluidic channel, the linear end-to-end model of the FMC is illustrated in Fig. 4. Using the developed system-theoretic model, we incorporate the noise and the memory effects into a linear end-to-end signal model. The linear received signal model for the molecular receiver is formulated as

$$\begin{aligned} \chi &= \alpha_{rx} (\alpha_{ch} (\alpha_{tx} \varphi + n_{tx}) + n_{ch}) + n_{rx} \\ &= \alpha_{e2e} \varphi + n_{e2e} \end{aligned} \quad (25)$$

where φ and χ are the magnitudes of the transmitted and received signals, i.e., $\varphi = |\Phi_+(k_0)|$ and $\chi = |\Phi_-(k_0)|$, respectively; α_{e2e} is the end-to-end signal gain given by $\alpha_{tx}\alpha_{ch}\alpha_{rx}$;

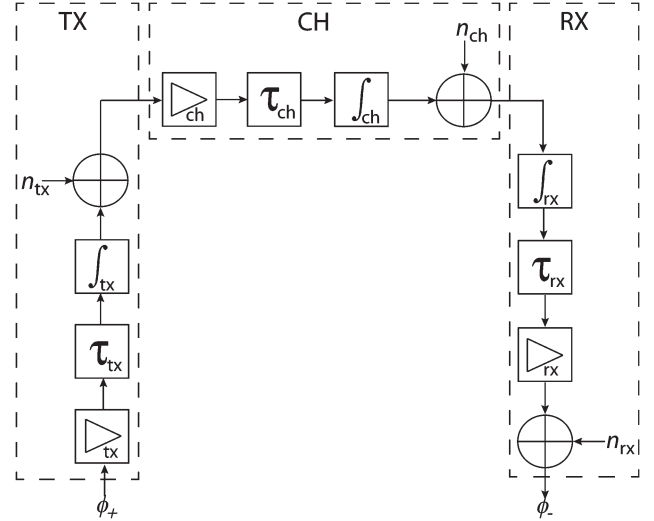


Fig. 4. Block diagram representation of the linear end-to-end signal model.

n_{tx} , n_{ch} , and n_{rx} are the noise effects at the output of the transmitter chamber, microfluidic channel, and receiver chamber; n_{e2e} is the end-to-end noise term given by

$$n_{e2e} = \alpha_{rx}\alpha_{ch}n_{tx} + \alpha_{rx}n_{ch} + n_{rx}. \quad (26)$$

Incorporating the transmitter and the receiver chamber delays, the end-to-end delay is formulated as

$$\tau_{e2e} = \tau_{rx} + \frac{a_{rx}}{2u} + \tau_{ch} + \frac{a_{tx}}{2u} + \tau_{tx} \quad (27)$$

where $a_{tx}/(2u)$ and $a_{rx}/(2u)$ are the delays added to provide causality for the transmitter and the receiver chamber impulse responses. We add these delays into τ_{ch} to incorporate into travel time inside microfluidic channel, and define the extended microfluidic channel delay τ_{ch}^* as

$$\tau_{ch}^* = \tau_{ch} + \frac{a_{tx} + a_{rx}}{2u}. \quad (28)$$

The memory effects due to diffusion of previously transmitted molecular signals inside microfluidic channel and chambers will be elaborated and incorporated into linear end-to-end model in Section V. Next, we derive the building blocks of the propagation noise, and investigate the spectral density of the end-to-end propagation noise on the received concentration.

IV. PROPAGATION NOISE ANALYSIS

In this section, for the linear signal model in (25), the noise effects on the received concentration signal are characterized using the autocorrelation of the corresponding impulse responses of the transmitter chamber (14), the microfluidic channel (2), and the receiver chamber (17). To this end, first, building blocks of noise autocorrelations are defined based on the propagation of the concentration signal by diffusion and at the junction transition, which are similar to thermal and shot noise effects, respectively, in electronic circuits. Then, autocorrelation of the propagation noise at the chambers and the microfluidic channel are formulated. Finally, spectral density of the end-to-end propagation noise is obtained, and statistical properties are studied.

A. Building Blocks of the Molecular Noise

The molecules forming a concentration signal are under continuous displacement due to the Brownian motion. Therefore, discrete and independent motion of molecules results in a non-continuous concentration signal, and the molecules passing at the junction between the microfluidic channel and the chambers vary in an unpredictable way. Diffusion noise defined as the noise effect due to Brownian motion of the molecules during diffusion-based and convection-based transport of molecules. Junction transition noise is observed when the molecules are transported by the flow in the only one direction. The molecular propagation at the junctions between the chambers and the microfluidic channel are exposed to such noise effects. In the following subsections, to characterize the propagation noise effects, autocorrelation functions of the diffusion noise and the junction transition noise, i.e., R_{diff} and R_{jct} , are formulated as the building blocks of the propagation noise at the chambers and the microfluidic channel.

1) *Diffusion Noise Autocorrelation Function:* For the diffusion noise, using the given solutions of the diffusion equation for the transmitter and receiver chambers in (8) and (16), respectively, we define the generalized impulse response of the propagation by diffusion as

$$h_{\text{diff}}(l) = \frac{1}{\sqrt{4\pi D_0 \tau_{\text{diff}}}} e^{-\frac{l^2}{4D_0 \tau_{\text{diff}}}} \quad (29)$$

where τ_{diff} is the diffusion duration. The autocorrelation of the concentration signal for the diffusion noise is given by

$$R_{\text{diff}}(\xi) = (\phi_{-}(l) * \phi_{-}(-l))(\xi) \quad (30)$$

where $\phi_{-}(l) = (h_{\text{diff}} * \phi_{+})(l)$. For an input concentration of $\phi_{+}(l) = \delta(l)$, the autocorrelation function of the diffusion noise is obtained as

$$\begin{aligned} R_{\text{diff}}(\xi) &= \int_{-\infty}^{\infty} h_{\text{diff}}(l + \xi) h_{\text{diff}}(l) dl \\ &= \frac{1}{\sqrt{8\pi D_0 \tau_{\text{diff}}}} e^{-\frac{\xi^2}{8D_0 \tau_{\text{diff}}}}. \end{aligned} \quad (31)$$

Furthermore, spectral density of diffusion noise is given by $\mathcal{F}\{R_{\text{diff}}\}$ as

$$S_{\text{diff}}(k) = e^{-2k^2 D_0 \tau_{\text{diff}}}. \quad (32)$$

2) *Junction Transition Noise Autocorrelation Function:* Based on impulse responses of the transmitter and the receiver junctions, i.e., $h_{\text{jct}}^{\text{tx}}$ and $h_{\text{jct}}^{\text{rx}}$, respectively, a generic impulse response is defined as

$$h_{\text{jct}}(l) = \frac{1}{a_{\text{jct}}} \text{rect}\left(\frac{l}{a_{\text{jct}}}\right) \quad (33)$$

where a_{jct} is the chamber height. Similar to the calculation of the autocorrelation function R_{diff} for diffusion noise in (30), the autocorrelation of junction transition noise R_{jct} is given by

$$R_{\text{jct}}(\xi) = (\phi_{-}(l) * \phi_{-}(-l))(\xi) \quad (34)$$

where concentration signal $\phi_{-}(l) = (h_{\text{jct}} * \phi_{+})(l)$. For an input signal of $\phi_{+}(l) = \delta(l)$, R_{jct} is found as

$$\begin{aligned} R_{\text{jct}}(\xi) &= \int_{-\infty}^{\infty} h_{\text{jct}}(l + \xi) h_{\text{jct}}(l) dl \\ &= \frac{1}{a_{\text{jct}}^2} \int_{-\infty}^{\infty} \text{rect}\left(\xi + \frac{l}{a_{\text{jct}}}\right) \text{rect}\left(\frac{l}{a_{\text{jct}}}\right) dl \end{aligned} \quad (35)$$

which is evaluated as

$$R_{\text{jct}}(\xi) = \begin{cases} \frac{1}{a_{\text{jct}}} - \frac{|\xi|}{a_{\text{jct}}^2}, & |\xi| \leq a_{\text{jct}} \\ 0, & \text{otherwise.} \end{cases} \quad (36)$$

Furthermore, the spectral density for the junction transition noise is found via Fourier Transform of the autocorrelation function $\mathcal{F}\{R_{\text{jct}}\}$ as

$$\begin{aligned} S_{\text{jct}}(k) &= \text{sinc}^2\left(\frac{a_{\text{jct}} k}{2\pi}\right) \\ &= \frac{\sin^2(a_{\text{jct}} k/2)}{a_{\text{jct}}^2 k^2/4}. \end{aligned} \quad (37)$$

B. Autocorrelation Analysis

Here, we formulate the autocorrelation of the propagation noise at the transmitter chamber, the microfluidic channel, and the receiver chamber using the developed building blocks of the propagation noise in the previous subsection.

1) *Transmitter Chamber:* The noise variance in the transmitter chamber is given by the diffusion of the transmitted concentration as

$$\begin{aligned} \Lambda_{\text{tx}}^2 &= (1 - \exp(-2k_0^2 D_0 \tau_{\text{tx}})) \psi^2 \\ &\approx (1 - (-2k_0^2 D_0 \tau_{\text{tx}} + 1)) \psi^2 \\ &= 2k_0^2 D_0 \tau_{\text{tx}} \psi^2 \end{aligned} \quad (38)$$

where the Taylor series expansion of $\exp(x) \approx x + 1$ for $x \approx 0$ is used. Combining the Fourier Transform of the diffusion and junction transition autocorrelation functions in (32) and (37), respectively, the spectral density of the transmitter chamber noise is obtained as

$$\begin{aligned} S_{\text{tx}}(k) &= \Lambda_{\text{tx}}^2 S_{\text{diff}}^{\text{tx}}(k) S_{\text{jct}}^{\text{tx}}(k) \\ &= 2k_0^2 D_0 \tau_{\text{tx}} \psi^2 e^{-2k^2 D_0 \tau_{\text{tx}}} \text{sinc}^2\left(\frac{a_{\text{tx}} k}{2\pi}\right) \end{aligned} \quad (39)$$

where $S_{\text{diff}}^{\text{tx}}$ and $S_{\text{jct}}^{\text{tx}}$ are the Fourier Transform of the autocorrelation of diffusion and junction transition adjusted to the transmitter chamber parameters.

2) *Microfluidic Channel:* Diffusion of the concentration signal through microfluidic channel gives the noise variance in the microfluidic channel as

$$\begin{aligned} \Lambda_{\text{ch}}^2 &= \alpha_{\text{tx}}^2 \left(1 - \exp(-2k_0^2 D_0 \tau_{\text{ch}}^*) \text{sinc}^2\left(\frac{a_{\text{ch}} \theta}{2\pi} k_0\right)\right) \psi^2 \\ &\approx \alpha_{\text{tx}}^2 \psi^2 + \alpha_{\text{tx}}^2 k_0^2 D_0 \tau_{\text{ch}}^* \text{sinc}^2\left(\frac{a_{\text{ch}} \theta}{2\pi} k_0\right) \psi^2 \\ &\quad - \alpha_{\text{tx}}^2 \text{sinc}^2\left(\frac{a_{\text{ch}} \theta}{2\pi} k_0\right) \psi^2 \end{aligned} \quad (40)$$

where the Taylor series expansion of $\exp(x) \approx x + 1$ for $x \approx 0$ is used. The spectral density of the straight microfluidic channel, i.e., $\theta = 0$, is as

$$S_{\text{ch}}(k) = \Lambda_{\text{ch}}^2 S_{\text{diff}}^{\text{ch}}(k) \quad (41)$$

where $S_{\text{diff}}^{\text{ch}}$ is the Fourier Transform of the autocorrelation of diffusion noise adjusted to microfluidic channel parameters, which is given by

$$S_{\text{diff}}^{\text{ch}}(k) = \alpha_{\text{tx}}^2 2k_0^2 D \tau_{\text{ch}}^* \psi^2 e^{-2k^2 D \tau_{\text{ch}}}. \quad (42)$$

3) *Receiver Chamber*: Diffusion of the concentration signal in the receiver chamber gives the receiver chamber noise variance as

$$\begin{aligned} \Lambda_{\text{rx}}^2 &= \alpha_{\text{tx}}^2 \alpha_{\text{ch}}^2 (1 - \exp(-2k_0^2 D_0 \tau_{\text{rx}})) \psi^2 \\ &\approx \alpha_{\text{tx}}^2 \alpha_{\text{ch}}^2 2k_0^2 D_0 \tau_{\text{rx}} \psi^2 \end{aligned} \quad (43)$$

where the Taylor series expansion of $\exp(x) \approx x + 1$ for $x \approx 0$ is used. Combining the Fourier Transform of the diffusion and junction transition noise autocorrelation functions in (32) and (37), respectively, the spectral density of the receiver chamber noise is obtained as

$$\begin{aligned} S_{\text{rx}}(k) &= \Lambda_{\text{rx}}^2 S_{\text{diff}}^{\text{rx}}(k) S_{\text{jct}}^{\text{rx}}(k) \\ &= \alpha_{\text{tx}}^2 \alpha_{\text{ch}}^2 2k_0^2 D_0 \tau_{\text{rx}} \psi^2 e^{-2k^2 D \tau_{\text{rx}}} \text{sinc}^2\left(\frac{a_{\text{rx}}}{2\pi} k\right) \end{aligned} \quad (44)$$

where $S_{\text{diff}}^{\text{rx}}$ and $S_{\text{jct}}^{\text{rx}}$ are the Fourier Transform of the autocorrelation of diffusion and junction transition adjusted to receiver chamber parameters.

C. The Noise Model for FMC

Here, we investigate the spectral densities of the three propagation noises, i.e., transmitter chamber noise n_{tx} , microfluidic channel noise n_{ch} , and the receiver chamber noise n_{rx} . In Fig. 5(a) and (b), the normalized chamber noise spectral density is depicted for various chamber length $l_{\text{tx}/\text{rx}}$ and chamber height $a_{\text{tx}/\text{rx}}$ values, respectively. It is shown that for sufficiently small wave number k , noise CSD can be taken as flat-band for transmitter and receiver chamber noises. Due to flat-band noise spectral density, the amplitude of the propagation noise can be taken as Gaussian distributed for the transmitter and receiver chambers. For the transmitter chamber noise, probability distribution is given by

$$n_{\text{tx}} \sim \mathcal{N}(0, \Lambda_{\text{tx}}^2) \quad (45)$$

where Λ_{tx}^2 is the transmitter chamber noise variance given by

$$\Lambda_{\text{tx}}^2 = 2k_0^2 D_0 \tau_{\text{tx}} \psi^2. \quad (46)$$

For the receiver chamber noise, probability distribution is given by

$$n_{\text{rx}} \sim \mathcal{N}(0, \Lambda_{\text{rx}}^2) \quad (47)$$

where Λ_{rx}^2 is the receiver chamber noise variance given by

$$\Lambda_{\text{rx}}^2 = 2k_0^2 D_0 \tau_{\text{rx}} \alpha_{\text{ch}}^2 \alpha_{\text{tx}}^2 \psi^2. \quad (48)$$

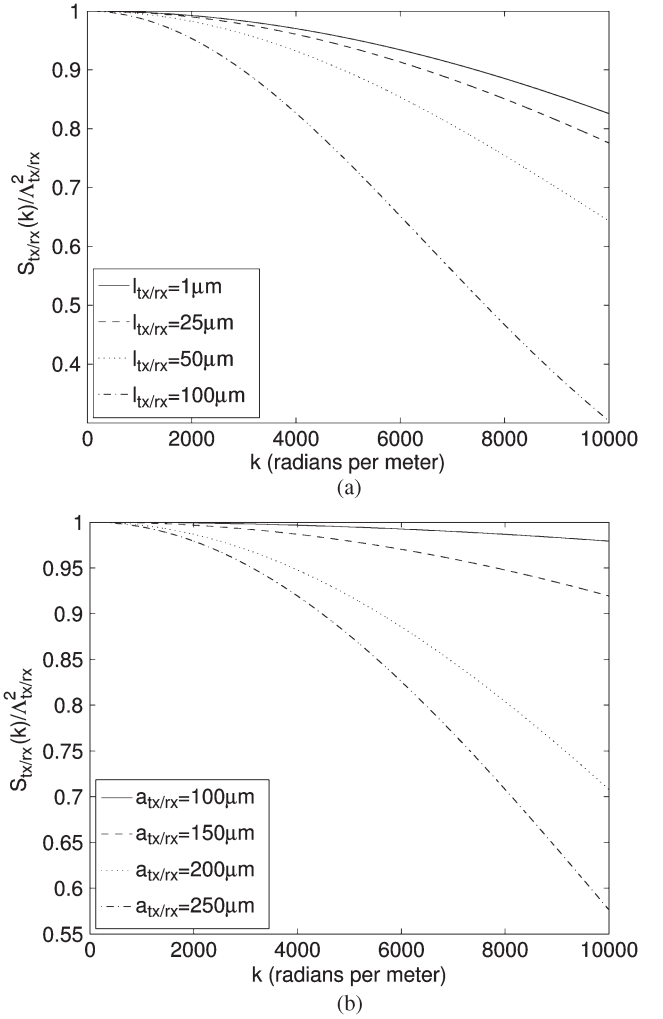


Fig. 5. Transmitter and receiver chamber noise spectral densities for various chamber length $l_{\text{tx}/\text{rx}}$ (a) and chamber height $a_{\text{tx}/\text{rx}}$ (b) values.

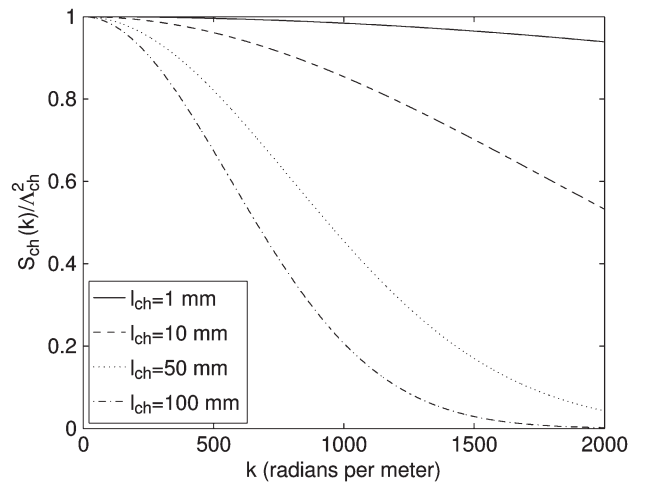


Fig. 6. Spectral density of the microfluidic channel noise for various length l_{ch} values.

Furthermore, in Fig. 6, it is shown that the spectral density of the noise at microfluidic channel can be taken as a flat-band for sufficiently small k values. Therefore, the amplitude

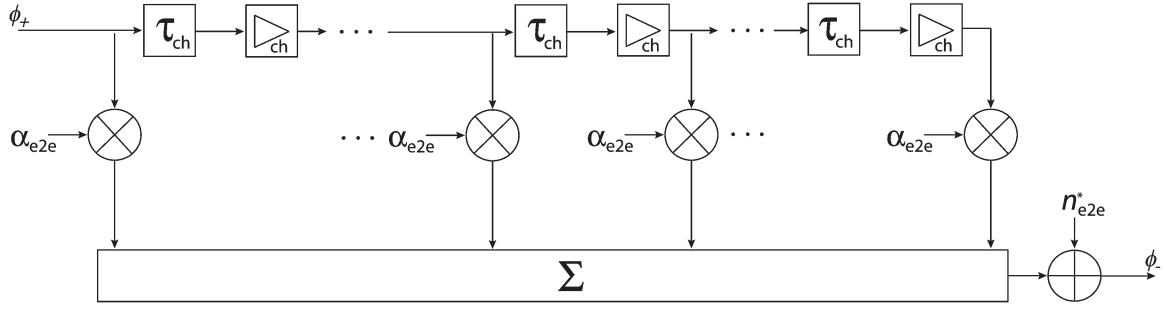


Fig. 7. Block diagram representation of the linear memory model.

distribution of the microfluidic channel noise can also be taken as Gaussian, i.e.,

$$n_{ch} \sim \mathcal{N}(0, \Lambda_{ch}^2) \quad (49)$$

where Λ_{ch}^2 is the microfluidic channel noise variance and can be approximated for a straight microfluidic channel as

$$\Lambda_{ch}^2 = 2k_0^2 D \tau_{ch}^* \alpha_{tx}^2 \psi^2. \quad (50)$$

Therefore, the end-to-end propagation noise can be approximated as Additive White Gaussian Noise (AWGN) based on the chamber and microfluidic channel parameters. Based on the end-to-end model given in (26), the distribution of the end-to-end propagation noise is obtained as

$$\begin{aligned} n_{e2e} &\sim \alpha_{rx} \alpha_{ch} n_{tx} + \alpha_{rx} n_{ch} + n_{rx} \\ &\sim \mathcal{N}(0, \Lambda_{e2e}^2) \end{aligned} \quad (51)$$

where Λ_{e2e}^2 is the variance of the end-to-end propagation noise and is given by

$$\Lambda_{e2e}^2 = 2k_0^2 (D_0 \tau_{tx} \alpha_{ch} \alpha_{rx}^2 + \alpha_{tx}^2 D \tau_{ch}^* \alpha_{rx}^2 + \alpha_{tx}^2 \alpha_{ch}^2 D_0 \tau_{rx}) \psi^2. \quad (52)$$

Since the frequency range of the flat-band noise spectral density is much smaller for microfluidic channel noise compared to the chamber noises, we will further investigate the frequency ranges where the end-to-end propagation noise spectral density is flat-band in Section VI-B for various microfluidic channel lengths, turning angles, and pressure drop values. Next, we investigate the memory effects in FMC.

V. MEMORY ANALYSIS

Memory effect is caused by the self-interference of the molecular signal through the transmitter/receiver chambers and microfluidic channel due to the diffusion of the transmitted signal. In this section, we present a linear model of memory for FMC. Furthermore, we also investigate the effect of memory on the end-to-end propagation noise. Finally, we present the end-to-end signal model with memory.

A. Linear Memory Model

The transmitted signal diffuses throughout the transmitter chamber, microfluidic channel, and receiver chamber, respectively. Therefore, when the transmission wave number is sufficiently large, transmitted signal will be exposed to the

self-interference. For transmission wave number k_0 , required propagation time for channel memory τ_{mem} is defined equal to period of the transmitted signal as

$$\begin{aligned} \tau_{mem} &= \frac{1}{f_0} \\ &= \frac{2\pi}{k_0 u} \end{aligned} \quad (53)$$

where identity $ku = 2\pi f$ for molecular signals is used [12]. When propagation time is higher than the τ_{mem} , the received signal becomes exposed to the memory. The linear memory model is given in Fig. 7. Based on the wave number k and the distance, the multiple memory branches may become active. The memory coefficient $\beta_{tx/rx}$ for transmitter/receiver chambers is defined as

$$\beta_{tx/rx} = e^{(-k_0 D_0 \frac{2\pi}{u})} \quad (54)$$

and the memory coefficient β_{ch} for microfluidic channel is defined as

$$\beta_{ch} = e^{(-k_0 D \frac{2\pi}{u})}. \quad (55)$$

The memory is composed of three parts, i.e., the transmitter chamber, the microfluidic channel, and the receiver chamber, as

$$I = I_{rx} + I_{ch} + I_{tx}. \quad (56)$$

For the memory at the chambers, required condition on channel for memory is given by

$$\tau_{mem} < \tau_{tx/rx}. \quad (57)$$

Accordingly, the memory level, i.e., the number of active branches in the presented model shown in Fig. 7, is given by

$$\eta_{tx/rx} = \left\lfloor \frac{\tau_{tx/rx}}{\tau_{mem}} \right\rfloor. \quad (58)$$

For the memory at the microfluidic channel, required condition for memory is given by

$$\tau_{mem} < \tau_{ch}. \quad (59)$$

Accordingly, the memory level at the microfluidic channel is equal to

$$\eta_{ch} = \left\lfloor \frac{\tau_{ch}}{\tau_{mem}} \right\rfloor. \quad (60)$$

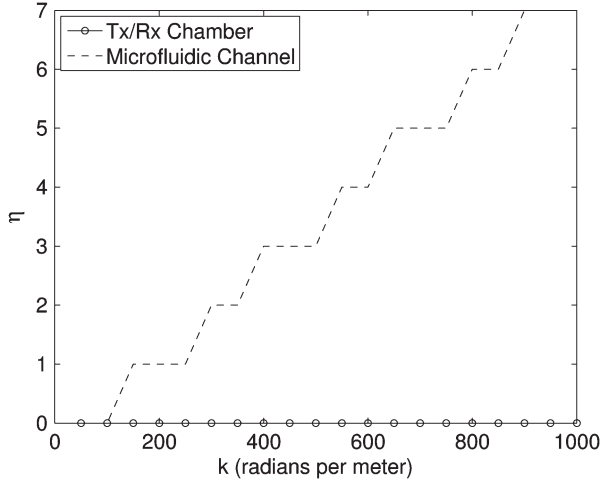


Fig. 8. Memory level at transmitter/receiver chambers $\eta_{tx/rx}$ and microfluidic channels η_{ch} versus the wave number k .

In Fig. 8, memory level for chambers and microfluidic channel is presented with respect to the transmission frequency. For numerical results, chamber length $l_{tx/rx}$ is $1 \mu\text{m}$, flow velocity is 10^{-4} m/s , and the microfluidic channel length l_{ch} is taken as 50 mm . It is observed that memory level $\eta_{tx/rx}$ is 0 for the whole frequency ranges of interest, meanwhile the memory level for the microfluidic channel η_{ch} increases with frequency as a step function and enables more memory branches at the microfluidic channel. Therefore, the end-to-end memory magnitude in (56) can be approximated based on the microfluidic channel memory as

$$I \approx I_{ch}. \quad (61)$$

Based on the end-to-end signal model given in (25), magnitude of the memory component in received molecular signal is given by

$$\begin{aligned} I &= \sum_{i=1}^{\eta_{ch}} \alpha_{rx} \beta_{ch}^i \alpha_{ch} \alpha_{tx} \varphi \\ &= \alpha_{rx} \alpha_{ch} \alpha_{tx} \frac{e^{-k_0 D \frac{\pi}{u}} - e^{-k_0 D \frac{2\pi}{u} (\eta_{ch} + 1)}}{1 - e^{-k_0 D \frac{2\pi}{u}}} \varphi. \end{aligned} \quad (62)$$

Furthermore, the variance of the memory component in the received molecular signal is given by

$$\begin{aligned} E[I^2] &= \sum_{i=1}^{\eta_{ch}} \alpha_{rx}^2 \beta_{ch}^{2i} \alpha_{ch}^2 \alpha_{tx}^2 \psi^2 \\ &= \alpha_{rx}^2 \alpha_{ch}^2 \alpha_{tx}^2 \frac{e^{-2k_0 D \frac{2\pi}{u}} - e^{-2k_0 D \frac{2\pi}{u} (\eta_{ch} + 1)}}{1 - e^{-2k_0 D \frac{2\pi}{u}}} \psi^2. \end{aligned} \quad (63)$$

Next, we continue our memory analysis with the effect of memory on the end-to-end molecular propagation noise.

B. End-to-End Propagation Noise Due to Memory

In addition to the memory model presented in the previous subsection, the end-to-end propagation noise variance is further amplified due to the self-interference of the transmitted signal molecules at the transmitter/receiver chambers and the microfluidic channel. Since the memory level at the chambers is

shown to be taken as 0 in the previous subsection, to incorporate the effect of memory into the end-to-end propagation noise, we use the definition of the microfluidic channel noise in Section IV-B2. For a τ_{mem} satisfying (59), the noise variance due to memory is found as

$$\begin{aligned} \Lambda_{MEM}^2 &= \sum_{i=1}^{\eta_{ch}} \alpha_{tx}^2 (1 - \alpha_{ch}^2 \beta_{ch}^{2i}) \alpha_{rx}^2 \psi^2 \\ &= \sum_{i=1}^{\eta_{ch}} \alpha_{tx}^2 \left(1 - e^{-2k_0^2 D (\tau_{ch} + \frac{1}{f_c} i)}\right) \alpha_{rx}^2 \psi^2 \\ &\approx \alpha_{tx}^2 \alpha_{rx}^2 2k_0^2 D \left(\eta \tau_{ch} + \frac{\eta(\eta+1)}{2f_0}\right) \psi^2 \end{aligned} \quad (64)$$

where the first order Taylor series expansion of $\exp(x) \approx x + 1$ for $x \approx 0$ is used.

Furthermore, similar to the microfluidic channel noise spectral density, the spectral density of the propagation noise due to memory is obtained as

$$\begin{aligned} S_{MEM}(k) &= \Lambda_{MEM}^2 S_{diff}^{ch}(k) \\ &= \alpha_{tx}^2 \alpha_{rx}^2 k_0^2 D \left(2\eta \tau_{ch} + \frac{\eta(\eta+1)}{f_0}\right) \psi^2 e^{-2k^2 D \tau_{ch}}. \end{aligned} \quad (65)$$

The noise spectral density with memory, i.e., spectral density of the unified end-to-end propagation noise, can also be taken as flat-band for sufficiently small k . Therefore, the unified end-to-end propagation noise n_{e2e}^* can be taken as Gaussian distributed. Based on the end-to-end model given in (26), the distribution of the unified end-to-end propagation noise is found as

$$n_{e2e}^* \sim \mathcal{N}(0, \Lambda_{e2e}^2 + \Lambda_{MEM}^2). \quad (66)$$

C. End-to-End Signal Model With Memory

The tapped delay-line model of molecular memory is illustrated in Fig. 7. The linear end-to-end model in (25) can be rearranged using (62) and (66) as

$$\begin{aligned} \chi &= \alpha_{rx} \alpha_{ch} \alpha_{tx} \varphi + n_{e2e}^* + I \\ &= \left(\frac{1 - e^{-k_0 D \frac{2\pi}{u} (\eta_{ch} + 1)}}{1 - e^{-k_0 D \frac{2\pi}{u}}} \right) \alpha_{rx} \alpha_{ch} \alpha_{tx} \varphi + n_{e2e}^*. \end{aligned} \quad (67)$$

Overall, the performed analyses for the end-to-end propagation noise and molecular memory provide an analytical framework to devise communication schemes for molecular communication over the microfluidic channels. Furthermore, the noise and memory models presented here complement the propagation analysis in [12].

VI. NUMERICAL RESULTS

In this section, obtained analytical results are numerically elaborated. We, first, study the signal propagation at the transmitter and receiver chambers. Specifically, we investigate the

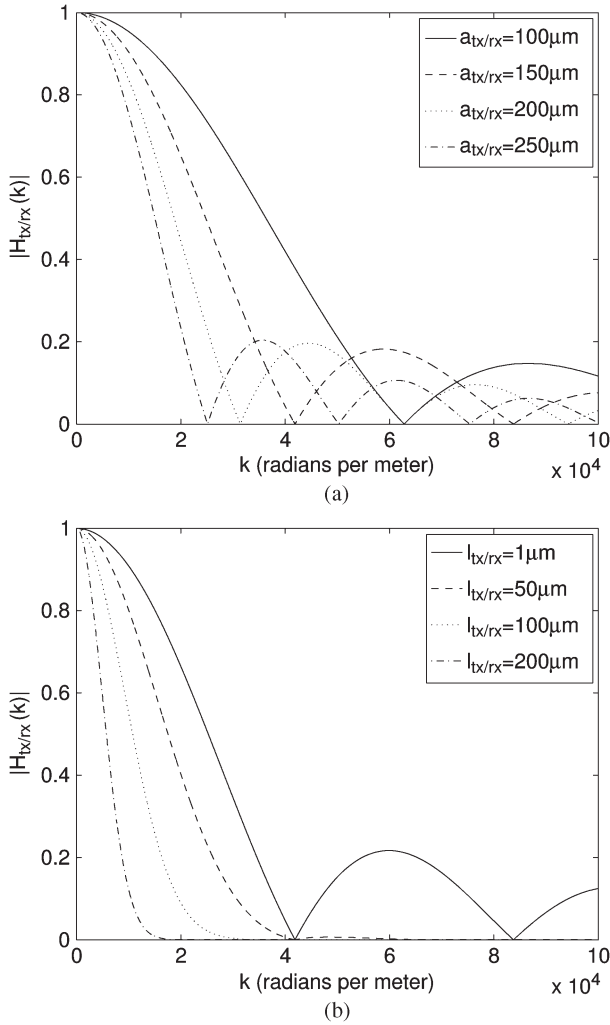


Fig. 9. Chamber attenuation based on chamber height $a_{tx/rx}$ (a) and chamber length $l_{tx/rx}$ (b).

effect of the chamber height and length for the transmitter and receiver chambers in Fig. 9(a) and (b). Then, we investigate the CSD of end-to-end propagation noise for microfluidic channel length l_{ch} , turning angle θ , and pressure drop Δp in Figs. 10(a), (b), and 11, respectively. During numerical evaluations, viscosity μ of the fluid is set to $10^{-3} \text{Pa} \cdot \text{s}$, and diffusion constant D_0 is set to $10 \cdot 10^{-10} \text{m}^2/\text{s}$.

A. Attenuation at the Transmitter and Receiver Chambers

The concentration propagation in chambers is studied in two parts, i.e., chamber height and length. To elaborate effect of chamber height $a_{tx/rx}$, chamber transfer function is investigated for channel length l_{ch} of $10 \mu\text{m}$ with respect to various chamber heights from $100 \mu\text{m}$ to $250 \mu\text{m}$ in Fig. 9(a). To illustrate the effect of chamber length $l_{tx/rx}$, chamber transfer function is investigated for a chamber height $a_{tx/rx}$ of $150 \mu\text{m}$ with respect to various chamber lengths from $1 \mu\text{m}$ to $200 \mu\text{m}$ in Fig. 9(b).

In Fig. 9(a), it is observed that as the chamber height decreases, i.e., for a shorter chamber height, the signal is exposed to less attenuation. The concentration signals with higher

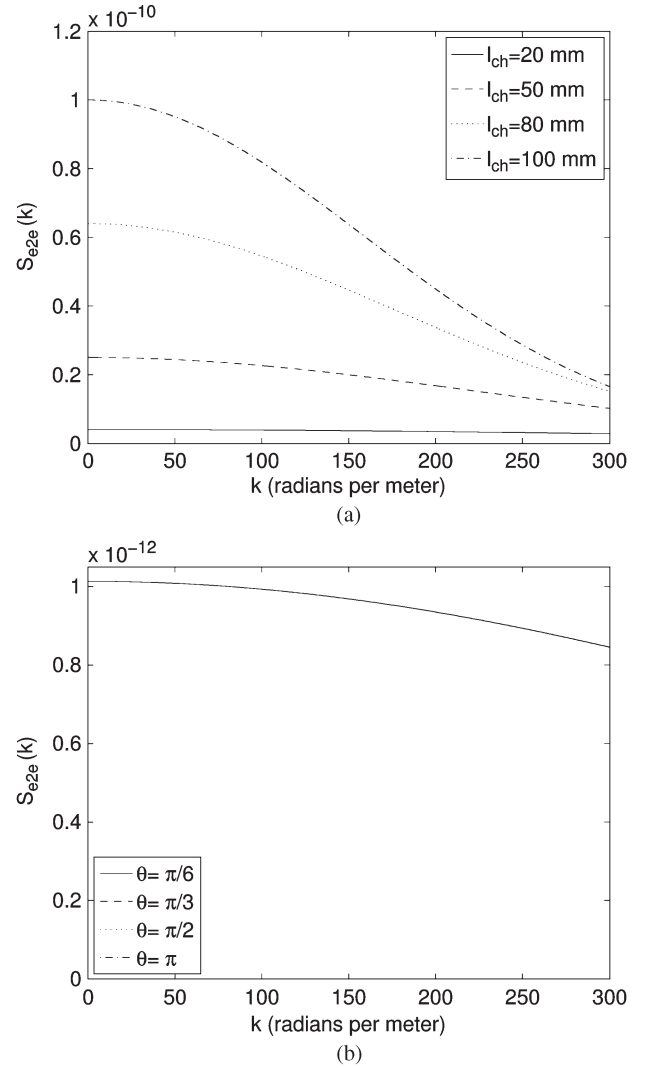


Fig. 10. The end-to-end propagation noise CSD based on length l_{ch} (a) and turning angle θ (b).

frequency can be transported with less attenuation at the transition junction from/to the shorter height chambers to/from microfluidic channel compared to the longer height chambers. In Fig. 9(b), when the chamber length is decreased from $200 \mu\text{m}$ to $1 \mu\text{m}$, the achievable frequencies are decreased as well. While $l_{tx/rx}$ is equal to 50 , 100 , and $200 \mu\text{m}$ attenuation due to diffusion dominates and junction transition effect is negligible, however, for $l_{tx/rx} = 1 \mu\text{m}$, attenuation due to junction transition outweighs the diffusion attenuation.

Overall, the chamber transfer function is equal to 0 when the wave number k is a positive integer, i.e., i , multiple of the reciprocal of the chamber height, i.e., $1/(a_{tx/rx})$, as

$$k = \frac{1}{a_{tx/rx}} i. \quad (68)$$

This effect is peculiar to the concentration propagation at the chamber junction, and it is due to the transition that cancel out the frequency components given by (68) at the output signal. To explain quantitatively, the chamber junction transition performs the integration of the input signal, and since the integration of a sinusoidal signal over a complete period, or the multiple

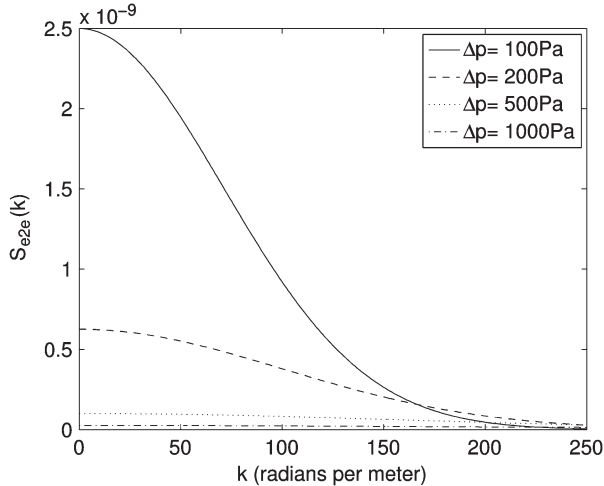


Fig. 11. The end-to-end propagation noise CSD based on the pressure drop across the microfluidic channel.

complete periods would yield 0, the frequency components matching this definition vanish, which are stated in (68).

B. End-to-End Propagation Noise

In Section IV-C, it is shown that the CSD of noise at microfluidic channel dominates the CSD of the noises at chambers. Therefore, the end-to-end propagation noise CSD is studied in three parts, i.e., the microfluidic channel length l_{ch} , the turning angle θ , and the pressure drop Δp . To elaborate effect of the microfluidic channel length l_{ch} , the end-to-end CSD is investigated for a pressure drop Δp of 500 Pa, height a_{ch} and width b_{ch} of 25 and 5 μm with respect to the various lengths from 20 mm to 100 mm in Fig. 10(a). To illustrate effect of the turning angle θ on the end-to-end noise CSD, l_{ch} is assumed as 100 mm, and the end-to-end CSD is investigated with respect to various turning angles from $\pi/6$ to π radians in Fig. 10(b). To illustrate effect of the pressure drop Δp on end-to-end noise CSD, end-to-end CSD is investigated with respect to various pressure drop values from 100 Pa to 1000 Pa in Fig. 11.

It is observed in Fig. 10(a) that as the distance between transmitter and receiver chambers increases, frequency range of the flat-band CSD decreases, i.e., as the microfluidic channel length decreases, the flat-band region of the end-to-end propagation noise CSD increases. Therefore, AWGN channel assumption for FMC holds for a limited range of frequencies based on the l_{ch} . Furthermore, the noise variance decreases by 10 times while the distance is decreased from 100 mm to 20 mm. Moreover, in Fig. 10(b), it is shown that turning channel effect is negligible for the end-to-end propagation noise CSD. In Fig. 11, it is shown that the flat-band region of end-to-end CSD increases from a few radians per meter to the order of 100 radians per meter, while pressure drop is increased from 100 to 1000 Pa. The end-to-end propagation noise variance is reduced while the pressure drop is increased from 100 to 1000 Pa, as well. Furthermore, these frequency ranges also conform with the biological oscillators based on quorum sensing [7]. Therefore, end-to-end propagation noise in FMC over microfluidic channels can be approximated as AWGN for microfluidic channels with sufficient channel length l_{ch} and pressure drop Δp .

Overall, the performed CSD analysis provides a basis for characterization of noise at the receiver based on the microfluidic channel parameters. Here, we focus on flat-band region, and the AWGN channel model for FMC over microfluidic channels. However, using proposed end-to-end propagation noise CSD, analysis of frequencies beyond flat-band region can also be performed for MC, such as colored noise models can be developed.

VII. CONCLUSION

In this paper, the propagation noise and memory analyses are performed for Flow-induced Molecular Communications (FMC). The objective of this work is the investigation of end-to-end propagation noise based on the chamber and microfluidic channel parameters. To the best of our knowledge, this is the first study of propagation noise in FMC. Motivated by the flat spectral density of the noise, an Additive White Gaussian Noise (AWGN) model is proposed for FMC. Furthermore, we model the molecular memory due to the inter-diffusion of transmitted concentration signals and show the effect of the memory on the propagation noise. We also investigate the signal propagation at the chambers, and the noise spectrum for various chambers, the microfluidic channel, and the transmission parameters.

The derived mathematical framework provides a complete analysis of the propagation characteristics for the combination of different mass transport phenomenons, i.e., diffusion in the chambers and convection in the microfluidic channels. Using developed building blocks for molecular noise, spectral density of the end-to-end propagation noise for any MC architecture can be analyzed. Accordingly, suitable noise model for the transmission frequency range of interest can be developed.

The memory effect is investigated from both impact of different molecular transport phenomenons and impact on molecular noise perspectives. Necessary conditions for memoryless MC are defined for both diffusion-based and convection-based molecular transport. Developed memory analysis for proposed microfluidic MC architecture can be applied to any combination of the molecular transport mechanisms as well.

Therefore, our analysis is universal, and independent of the microfluidic MC architecture. The developed linear end-to-end channel model sets the stage for capacity analysis, and design of complex modulation, coding, and receiver schemes for MC over microfluidic channels. On the other hand, to model generation of molecular signal and distortion effects on it, analysis and design biological transceivers are imperative as well.

REFERENCES

- [1] I. F. Akyildiz, J. M. Jornet, and M. Pierobon, "Nanonetworks: A new frontier in communications," *Commun. ACM*, vol. 54, no. 11, pp. 84–89, Nov. 2011.
- [2] I. F. Akyildiz, F. Brunetti, and C. Blazquez, "Nanonetworks: A new communication paradigm," *Comput. Netw. J.*, vol. 52, no. 12, pp. 2260–2279, Aug. 2008.
- [3] G. M. Whitesides, "The origins and the future of microfluidics," *Nature*, vol. 442, no. 7101, pp. 368–373, Jul. 2006.
- [4] H. A. Stone, A. D. Stroock, and A. Ajdari, "Engineering flows in small devices: Microfluidics toward a lab-on-a-chip," *Annu. Rev. Mech.*, vol. 36, pp. 381–411, Jan. 2004.
- [5] T. M. Squires and S. R. Quake, "Microfluidics: Fluid physics at the nanoliter scale," *Rev. Mod. Phys.*, vol. 77, no. 3, pp. 977–1026, Oct. 2005.

- [6] I. F. Akyildiz, F. Fekri, R. Sivakumar, C. R. Forest, and B. K. Hammer, "MONACO: Fundamentals of molecular nano-communication networks," *IEEE Wireless Commun.*, vol. 19, no. 5, pp. 12–18, Oct. 2012.
- [7] T. Danino, O. Mondragon-Palomino, L. Tsimring, and J. Hasty, "A synchronized quorum of genetic clocks," *Nature*, vol. 463, no. 7279, pp. 326–330, Jan. 2010.
- [8] M. Pierobon and I. F. Akyildiz, "End-to-end physical model of molecular communications," *IEEE J. Sel. Areas Commun.*, vol. 28, no. 4, pp. 602–611, May 2010.
- [9] T. Nakano and J.-Q. Liu, "Design and analysis of molecular relay channels: An information theoretic approach," *IEEE Trans. NanoBioscience*, vol. 9, no. 3, pp. 213–221, Sep. 2010.
- [10] M. Pierobon and I. F. Akyildiz, "Noise analysis in ligand-binding reception for molecular communication in nanonetworks," *IEEE Trans. Signal Process.*, vol. 59, no. 9, pp. 4168–4182, Sep. 2011.
- [11] M. Pierobon and I. F. Akyildiz, "Diffusion-based noise analysis for molecular communication in nanonetworks," *IEEE Trans. Signal Process.*, vol. 59, no. 6, pp. 2532–2547, Jun. 2011.
- [12] A. O. Bicen and I. F. Akyildiz, "System-theoretic analysis and least-squares design of microfluidic channels for flow-induced molecular communication," *IEEE Trans. Signal Process.*, vol. 61, no. 20, pp. 5000–5013, Oct. 2013.
- [13] K. W. Oh, K. Lee, B. Ahn, and E. P. Furlani, "Design of pressure-driven microfluidic networks using electric circuit analogy," *Lab Chip*, vol. 12, no. 3, pp. 515–545, Feb. 2012.
- [14] Y. Zhou, Y. Wang, T. Mukherjee, and Q. Lin, "Generation of complex concentration profiles by partial diffusive mixing in multi-stream laminar flow," *Lab Chip*, vol. 9, no. 10, pp. 1439–1448, May 2009.
- [15] S. K. Griffiths and R. H. Nilson, "Design and analysis of folded channels for chip-based separations," *Anal. Chem.*, vol. 74, no. 13, pp. 2960–2967, Jul. 2002.
- [16] S. K. Griffiths and R. H. Nilson, "Low-dispersion turns and junctions for microchannel systems," *Anal. Chem.*, vol. 73, no. 2, pp. 272–278, Jan. 2001.
- [17] Y. Wang, T. Mukherjee, and Q. Lin, "Systematic modeling of microfluidic concentration gradient generators," *J. Micromech. Microeng.*, vol. 8, no. 5, pp. 2128–2137, Oct. 2006.
- [18] A. S. Bedekar, Y. Wang, S. Krishnamoorthy, S. S. Siddhaye, and S. Sundaram, "System-level simulation of flow-induced dispersion in lab-on-a-chip systems," *IEEE Trans. Comput.-Aided Design Integr. Circuits Syst.*, vol. 25, no. 2, pp. 294–304, Feb. 2006.
- [19] S. Kim, H. J. Kimzb, and N. L. Jeon, "Biological applications of microfluidic gradient devices," *Integr. Biol.*, vol. 2, no. 11/12, pp. 584–603, Nov. 2010.
- [20] Y. Xie, Y. Wang, L. Chen, and C. H. Mastrangelo, "Fourier microfluidics," *Lab Chip*, vol. 8, no. 5, pp. 779–785, May 2008.
- [21] B. Atakan and O. B. Akan, "On channel capacity and error compensation in molecular communication," in *Transactions on Computational Systems Biology X*. Berlin, Germany: Springer-Verlag, 2008, pp. 59–80.
- [22] D. J. Spencer, S. K. Hampton, P. Park, J. P. Zurkus, and P. J. Thomas, "The diffusion-limited biochemical signal-relay channel," in *Proc. Adv. Neural Inf. Process. Syst.*, 2004, vol. 16, pp. 1–8.
- [23] M. J. Moore, T. Suda, and K. Oiwai, "Molecular communication: Modeling noise effects on information rate," *IEEE Trans. NanoBioscience*, vol. 8, no. 2, pp. 169–180, Jun. 2009.
- [24] B. Kirby, *Micro- and Nanoscale Fluid Mechanics: Transport in Microfluidic Devices*. New York, NY, USA: Cambridge University Press, 2010.
- [25] H. Bruus, *Theoretical Microfluidics*. London, U.K.: Oxford Univ. Press, 2008.
- [26] D. Dutta and D. T. Leighton, "Dispersion reduction in pressure-driven flow through microetched channels," *Anal. Chem.*, vol. 73, no. 3, pp. 504–513, Feb. 2001.



A. Ozan Bicen (S'08) received the B.Sc. degree in electrical and electronics engineering from Middle East Technical University, Ankara, Turkey, in 2010 and the M.Sc. degree in electrical and electronics engineering from Koç University, Istanbul, Turkey, in 2012. He is currently working toward the Ph.D. degree in the School of Electrical and Computer Engineering, Georgia Institute of Technology, Atlanta, GA, USA.

He is currently a Graduate Research Assistant with the Broadband Wireless Networking Laboratory, School of Electrical and Computer Engineering, Georgia Institute of Technology. His current research interests include design and analysis of molecular communication systems, cognitive radio networks, and wireless sensor networks.



Ian F. Akyildiz (M'86–SM'89–F'96) received the B.S., M.S., and Ph.D. degrees from the University of Erlangen-Nurnberg, Erlangen, Germany, in 1978, 1981, and 1984, respectively, all in computer engineering.

He is currently the Ken Byers Chair Professor in Telecommunications with the School of Electrical and Computer Engineering, Georgia Institute of Technology, Atlanta, GA, USA, the Director of the Broadband Wireless Networking Laboratory, and the Chair of the Telecommunication Group. He is an Honorary Professor with the School of Electrical Engineering, Universitat Politècnica de Catalunya (UPC) in Barcelona, Spain, and founded the NaNoNetworking Center in Catalunya (N3Cat). He is also an Honorary Professor with the Department of Electrical, Electronic and Computer Engineering, University of Pretoria, Pretoria, South Africa, and the Founder of the Advanced Sensor Networks Laboratory. Since September 2012, he has been a FiDiPro Professor (Finland Distinguished Professor Program (FiDiPro) supported by the Academy of Finland, Helsinki, Finland) at Department of Communications Engineering, Tampere University of Technology, Tampere, Finland. He is the Editor-in-Chief of *Computer Networks* (Elsevier) and the founding Editor-in-Chief of *Ad Hoc Networks* (Elsevier), *Physical Communication* (Elsevier), and *Nano Communication Networks* (Elsevier). His current research interests are in nanonetworks, Long Term Evolution (LTE) advanced networks, cognitive radio networks, and wireless sensor networks.

Prof. Akyildiz is a Fellow of the Association for Computing Machinery (ACM). He was the recipient of numerous awards from IEEE and ACM.